Bharat Laxmi[1], *Khem Chand*[1], *Pankaj Thakur*[2*]

ANALYSIS OF HEAT AND MASS TRANSFER IN HYDROMAGNETIC HYBRID NANOFLUID FLOW OVER A PERMEABLE STRETCHING/SHRINKING CYLINDER WITH THERMO-DIFFUSION EFFECTS

ANALIZA PRELAZA TOPLOTE I MASE U HIDROMAGNETNOM PROTOKU HIBRIDNOG NANOFLUIDA PREKO PROPUSNOG ISTEGNUTOG/SKUPLJENOG CILINDRA SA EFEKTIMA DIFUZIJE

Originalni naučni rad / Original scientific paper
Rad primljen / Paper received: 24.04.2025
https://doi.org/10.69644/ivk-2026-01-0139

Adresa autora / Author's address:
[1)] Department of Mathematics & Statistics, Himachal Pradesh University, Summer Hill, Shimla-171005, India
K. Chand https://orcid.org/0000-0002-6360-7729
[2)] Department of Mathematics, ICFAI University Baddi, Solan, Himachal Pradesh, India
P. Thakur https://orcid.org/0000-0001-8119-2697
[*]email: pankajthakur15@yahoo.co.in

Keywords
- hydromagnetic
- hybrid nanofluid
- stretching/shrinking cylinder
- thermo-diffusion effects
- suction

Ključne reči
- hidromagnetni
- hibridni nanofluid
- istezanje/skupljanje cilindra
- termodifuzioni efekti
- usisavanje

Abstract

This study aims to investigate the heat transfer properties of hydromagnetic hybrid nanofluid flow subjected to thermo-diffusion effects around a stretching/shrinking cylinder. In this study, alumina (Al_2O_3) and copper (Cu) nanoparticles are used as a hybrid nanofluid, while water (H_2O) acts as the base fluid. The governing nonlinear partial differential equations are transformed into linear ordinary differential equations using similarity transformations and are solved numerically by using the bvp4c function of MATLAB® software. This study analyses the effects of various physically controllable parameters, such as magnetic field, permeability parameter, Eckert number, Schmidt number, curvature parameter, Brownian motion parameter, thermophoresis parameter, stretching/shrinking, and suction/injection parameter on flow and heat transfer characteristics. The effects on these parameters, velocity, temperature, and concentration fields, have been graphically presented, and their physical interpretation has been provided. Additionally, the numerical solutions of key physical quantities, such as skin friction, Nusselt number, and Sherwood number, have been computed for various parameters and presented through graphs. The analysis shows that the magnetic field parameter has an opposite effect on the velocity profile. The temperature and concentration profiles also increase with the enhancement of the curvature parameter. It is also observed that the increase in hybrid nanofluid particles (Al_2O_3-Cu/H_2O) enhances the velocity, temperature, and concentration profiles.

Izvod

U rada je opisano istraživanje osobina prenosa toplote u hidromagnetnom protoku hibridnog nanofluida, na koji utiče termo-difuzija oko istegnutog/skupljenog cilindra. Koriste se nanočestice aluminijum oksida (Al_2O_3) i bakra (Cu) kao hibridni nanofluid, dok se voda (H_2O) ponaša kao bazni fluid. Osnovne nelinearne parcijalne diferencijalne jednačine se transformišu u obične linearne diferencijalne jednačine transformacijama sličnosti i rešavaju se numerički funkcijom bvp4c softvera MATLAB®. U radu se analiziraju uticaji raznih fizički upravljivih parametara, kao što su magnetno polje, parametar permeabilnosti, Ekertov broj, Šmitov broj, parametar krivine, parametar Braunovog kretanja, parametar termoforeze, istezanje/skupljanje, i parametar usisavanja/ubrizgavanja na karakteristike protoka i prelaza toplote. Za ove parametre grafički su predstavljeni uticaji brzine, temperature, koncentracije, i data je njihova fizička interpretacija. Osim toga, za razne parametre data su numerička rešenja i grafički su predstavljene ključne fizičke veličine, kao što su površinsko trenje Nuseltov broj i Šervudov broj. Analiza pokazuje da parametar magnetnog polja ima suprotan efekat na profil brzine. Profili temperature i koncentracije takođe rastu sa parametrom krivine. Takođe se primećuje da se sa porastom čestica hibridnog nanofluida (Al_2O_3-Cu/H_2O) povećavaju profili brzine, temperature i koncentracije.

INTRODUCTION

Researchers worldwide are deeply engaged in understanding ways to enhance heat transfer, particularly in boundary layer flow, which plays a crucial role in many industrial and scientific applications. The primary objective of this study is to understand how the fluid flowing near a solid surface affects its thermal properties, such as conductivity and heat capacity. The study of nanofluids in this direction has become extremely important. Nanofluids are specially engineered fluids that contain suspended nanoparticles ranging from 1 to 100 nanometres in size. These nanoparticles can be made from metals, oxides, carbides, or carbon nanotubes and are mixed with base fluids such as water, ethylene glycol, or oil. The main characteristic of nanofluids is their

significantly higher thermal conductivity compared to traditional base fluids, making them highly effective. Due to this property, the use of nanofluids is rapidly increasing in various fields, including microelectronics, fuel cells, medicinal processes, and engine design.

The concept of nanofluids, first introduced by Choi /1/ in 1995, has emerged as a more effective solution compared to traditional heat transfer fluids. Further, Choi et al. /2/ have used copper nanoparticles of size less than one percent to increase the poor thermal conductivity of the liquid, and they find better results of heat transfer. Another significant result in the field of nanofluid is obtained by Patel et al. /3/. They investigate the thermal conductivities of naked and monolayer-protected metal nanoparticles with anomalous and chemical effects. In recent years, nanofluids have attracted significant attention from researchers, as extraordinary improvements of their thermal properties are confirmed. The study of convective heat transfer in nanofluids is rapidly attracting the attention of researchers as they find widespread use in various industries. Due to the unique physical and chemical properties of nanoparticles in the nanometre size range, they are proving to be highly effective. The development of metal nanoparticle suspensions is also being pursued for other purposes, including medical fields, particularly therapeutic applications such as cancer therapy. The multidisciplinary nature of nanofluid research offers vast possibilities for new explorations and discoveries in the field of nanotechnology. By increasing the concentration of suspended nanoparticles, which often have higher thermal conductivity than the base fluid, significant improvements in heat transfer efficiency can be achieved.

Several researchers have explored the natural convection heat transfer of nanofluids in enclosures using numerical techniques. Abbas et al. /4/ conducted a numerical analysis of heat transfer in a viscous fluid over an unsteady stretching/shrinking cylinder with suction and partial slip. A unique solution was found for the stretching cylinder, whereas dual solutions are obtained for the shrinking cylinder. Hayat et al. /5/ investigated the heating effects of nanofluids induced by a permeable stretching cylinder using the Homotopy Analysis Method (HAM). Mittal et al. /6/ have briefly discussed the problem of rotationally oscillating circular cylinders in fluid dynamics. Bilal et al. /7/ conducted a numerical investigation on the effects of magnetohydrodynamics and thermal radiation on Williamson nanofluid flow over a stretching cylinder. They observed that as the Weissenberg number increases, the velocity profile decreases, while the temperature profile exhibits the opposite trend. Al-Mdallal et al. /8/ investigate unsteady viscous flow over a shrinking permeable cylinder saturated in a porous medium under the influence of a magnetic field. Khashi'ie et al. /9/ studied the thermally stratified flow of (Al_2O_3-Cu/H_2O) hybrid nanofluid near a permeable stretching/shrinking spherical cylinder. Nanofluid flow over a permeable stretching/shrinking cylinder is investigated by Roşca et al. /10/. They used the Buongiorno mathematical nanofluid model in their study. In a subsequent study, Mishra and Kumar /11/ investigate the flow and thermal characteristics of an MHD silver-water (Ag/H_2O) nanofluid over a stretching cylinder, considering suction/injection and slip boundary conditions. Their study includes Joule heating and viscous dissipation effects. They find a similar behaviour of the temperature profile concerning the dissipation and heat generation/absorption parameters.

Analysis of boundary layer flows in viscous fluids influenced by continuously moving or stretching/shrinking surfaces has significant applications in engineering processes and the polymer industry. Examples of such polymer-related technological processes include the cooling of continuous sheets or fibres, glass blowing, of continuous sheets or fibres, glass blowing, the continuous stretching of plastic films and synthetic fibres, continuous metal casting, fibre spinning, hot rolling, wire drawing, and paper manufacturing. Khan and Rasheed /12/ studied velocity and temperature slip effects on a hybrid nanofluid composed of molybdenum disulfide and silicon oxide near an irregular 3D surface. Kumar et al. /13/ focus on the behaviour of a ferrofluid flowing over a stretching cylinder, incorporating the effects of thermophoretic particle deposition. The study also considers the presence of a uniform heat source or sink. The primary objective was to understand how these factors influence the fluid flow and heat transfer characteristics, providing insights into controlling particle deposition in industrial processes. Arshad et al. /14/ investigates the impact of thermophoresis and the Brownian effect on a chemically reacting magnetohydrodynamics (MHD) nanofluid over an exponentially stretching sheet. Najib et al. /15/ investigate the flow and heat transfer behaviour at the stagnation point of a nanofluid surrounding an exponentially stretching/shrinking cylinder. The study accounts for boundary slip effects, which impact skin friction and heat transfer rates. Furthermore, the influence of various nanoparticles and their volume fractions is analysed, offering valuable insights into improving the thermal efficiency of nanofluid-based systems.

Sarkar and Das /16/ investigate the flow and heat transfer behaviour of a magneto-hybrid nanofluid around an impermeable stretching flexible cylinder, considering the effects of activation energy and chemical reaction. Khan et al. /17/ investigate the behaviour of MHD hybrid nanofluids in a stagnation-point flow towards a porous stretching cylinder under the influence of thermal radiation. By incorporating multiple types of nanoparticles, hybrid nanofluids are examined for their impact on flow dynamics and heat transfer characteristics. The presence of thermal radiation introduces additional complexity, making the study particularly relevant for high-temperature applications and modern cooling systems. These findings enhance the understanding of how nanoparticles, magnetic fields, and different boundary conditions affect fluid motion and thermal regulation. Such insights play a vital role in the advancement and optimisation of efficient thermal management strategies in engineering and industrial sectors. Li et al. /18/ study the heat transfer and flow behaviour of a hybrid nanofluid moving over a stretched cylinder at an oblique stagnation point, where the fluid impacts the surface at an angle. The flow is influenced by various changing factors, such as thermal properties, velocity, and external forces as magnetic fields. By combining different nanoparticles in the fluid, researchers analyse

how these variations affect heat transfer efficiency and fluid movement. The findings help in optimising cooling and thermal management in industrial and engineering applications.

Building on previous research, this study offers a theoretical investigation of hydromagnetic hybrid nanofluid flow over a permeable stretching/shrinking cylinder, considering thermo-diffusion effects. The hybrid nanofluid comprises alumina (Al_2O_3) and copper (Cu) nanoparticles suspended in a water-based fluid, enhancing thermal conductivity and fluid dynamics. The governing partial differential equations (PDEs) that describe the system are transformed into a set of nonlinear coupled ordinary differential equations (ODEs) using a suitable similarity transformation method. This transformation simplifies the mathematical model, making it more manageable for analysis and providing valuable insights into fluid flow and heat transfer behaviour. The transformed ODEs are numerically solved using the MATLAB bvp4c function which is designed for boundary value problems. The velocity and temperature field solutions are expressed in analytical form and then evaluated numerically using MATLAB. The study explores the influence of various parameters present in the governing equations, such as magnetic field, viscous dissipation, Brownian motion parameter, curvature parameter, and Schmidt number, on the velocity, temperature, and concentration profiles of the flow. These effects are visually represented through graphical plots to facilitate a comprehensive discussion on the flow characteristics and thermal behaviour under different conditions.

MATHEMATICAL FORMULATION

A steady incompressible hybrid nanofluid in the presence of a magnetic field, viscous dissipation, and heat source effect along a permeable deformable cylinder of radius a is considered. The cylindrical polar coordinates (r, x) are assigned in the radial and axial directions, respectively. The hybrid nanofluid flows in the axial x-direction, while the r-coordinate is normal to x, as illustrated in Fig. 1. The deformable cylinder has a linear velocity $U_w(x)$ with a constant characteristic velocity u_0 such that $U_w(x) = u_0x/L$. The wall mass transfer velocity is taken as $v_w(r) = -(a/r)S\sqrt{(u_0v_f/L)}$, where $S > 0$ denotes mass suction and $S < 0$, denotes mass injection. Here, $\lambda > 0$ represents the stretching constant, $\lambda < 0$ represents the shrinking constant, and $\lambda = 0$ corresponds to a motionless cylinder. The temperature of the fluid, $T_w(x) = T_\infty + T_0(x/L)^2$, is considered a nonlinear function of distance, where T_0 is a positive constant temperature of the fluid at the origin, and T_∞ is the free stream temperature of the fluid. Under the boundary layer approximation and the assumption of constant fluid properties, the continuity, momentum, and energy equations for the flow, following Khashi'ie et al. /9/ and Roşca et al. /10/, are as follows:

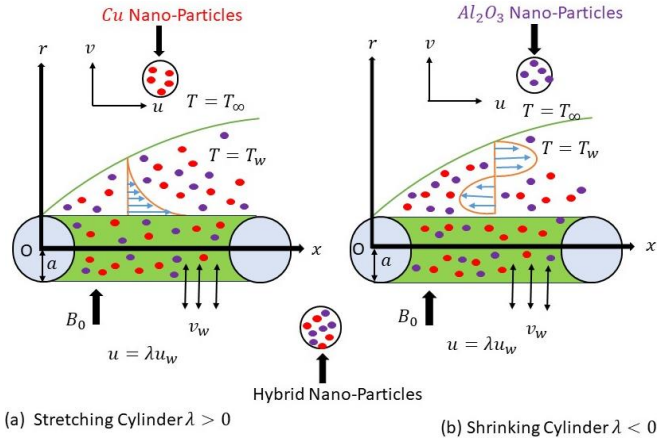

Figure 1. Physical model for stretching/shrinking cylinder.

$$\frac{\partial(ru)}{\partial x}+\frac{\partial(rv)}{\partial r}=0, \tag{1}$$

$$u\frac{\partial u}{\partial x}+v\frac{\partial u}{\partial r}=\frac{\mu_{hnf}}{\rho_{hnf}}\left(\frac{\partial^2 u}{\partial r^2}+\frac{1}{r}\frac{\partial u}{\partial r}\right)-\frac{\sigma_{hnf}}{\rho_{hnf}}B_0^2u-\frac{\mu_{hnf}}{\rho_{hnf}k'}u, \tag{2}$$

$$u\frac{\partial T}{\partial x}+v\frac{\partial T}{\partial r}=\frac{k_{hnf}}{(\rho c_p)_{hnf}}\left(\frac{\partial^2 T}{\partial r^2}+\frac{1}{r}\frac{\partial T}{\partial r}\right)+\frac{\sigma_{hnf}}{(\rho c_p)_{hnf}}B_0^2u+$$
$$+\delta\left[D_B\left(\frac{\partial C}{\partial r}\frac{\partial T}{\partial r}\right)+\left(\frac{D_T}{T_\infty}\right)\left(\frac{\partial T}{\partial r}\right)^2\right], \tag{3}$$

$$u\frac{\partial C}{\partial x}+v\frac{\partial C}{\partial r}=D_B\left(\frac{\partial^2 C}{\partial r^2}+\frac{1}{r}\frac{\partial C}{\partial r}\right)+\frac{D_T}{T_\infty}\left(\frac{\partial^2 T}{\partial r^2}+\frac{1}{r}\frac{\partial T}{\partial r}\right). \tag{4}$$

The boundary conditions for the present flow are given as follows:

$$u=U_w(x)\lambda,\quad v=v_0,\quad T=T_w,$$
$$D_B\frac{\partial C}{\partial r}+\frac{D_T}{T_\infty}\frac{\partial T}{\partial r}=0\quad\text{at}\quad r=au\to 0,$$
$$u=0,\quad T\to T_\infty,\quad C\to C_\infty\quad\text{as}\quad r\to\infty. \tag{5}$$

To transform governing equations into dimensionless form, we define the following similarity variables η, the dimensionless velocity variable f and temperature variable θ as:

$$u=\frac{u_0x}{L}f'(\eta),\quad v=-\frac{a}{r}\sqrt{\frac{u_0v_f}{L}}f(\eta),\quad \theta(\eta)=\frac{T-T_\infty}{T_w-T_\infty},$$
$$\phi(\eta)=\frac{C-C_\infty}{C_w-C_\infty},\quad \eta=\sqrt{\frac{u_0}{v_fL}}\frac{r^2-a^2}{2a}. \tag{6}$$

The transformed Eq.(6) satisfies the continuity Eq.(1). The equality can be used to convert the momentum and energy equations into related nonlinear ordinary differential equations using the dimensionless variables given in Eq.(6), resulting in Eqs.(2), (3), and (4) that are transformed as follows:

$$\left(\frac{\mu_{hnf}\rho_f}{\mu_f\rho_{hnf}}\right)[(1+2\gamma\eta)f'''+2\gamma f'']+ff''-f'^2-\left(\frac{\sigma_{hnf}\rho_f}{\sigma_f\rho_{hnf}}\right)Mf'-$$
$$-\left(\frac{\mu_{hnf}\rho_f}{\mu_f\rho_{hnf}}\right)Kf'=0, \tag{7}$$

$$\frac{1}{Pr}\frac{(\rho C_p)_f}{(\rho C_p)_{hnf}}\frac{k_{hnf}}{k_f}[(1+2\gamma\eta)\theta''+2\gamma\theta']+f\theta'+\frac{\sigma_{hnf}(\rho C_p)_f}{\sigma_f(\rho C_p)_{hnf}}\times$$
$$\times MEcf'^2+(1+2\gamma\eta)Nb\theta'\phi'+(1+2\gamma\eta)Nt\theta'^2=0, \tag{8}$$

$$(1+2\gamma\eta)\phi''+\left(\frac{Nt}{Nb}\right)[(1+2\gamma\eta)\theta''+2\gamma\theta']+2\gamma\phi'+Sc\phi' f=0. \tag{9}$$

From Eq.(5), the dimensionless boundary conditions are

$$f(0)=S,\ f'(0)=\lambda,\ \theta(0)=1,\ \text{at}\ \eta=0,\ Nb\phi'(0)+Nt\theta'(0)=0,$$
$$f'\to 0,\ \theta\to 0,\ \phi\to 0\ \text{as}\ \eta\to\infty, \tag{10}$$

where: $\gamma=\sqrt{(v_fL/u_0a^2)}$ is curvature parameter; $Pr=(\mu C_p)_f/k_f$ is Prandtl number; $M=\sigma_fB_0^2L/\rho_fu_0$ is magnetic field parameter; $K=\mu_fL/\rho_fk^*u_0$ is permeability parameter; $Ec=u_w^2/(T_w-$

$T_\infty)(C_p)_f$ is Eckert number (viscous dissipation); $Nb = (\rho c_p)_p \cdot D_B(C_w - C_\infty)/\nu(\rho c_p)_f$ is Brownian motion parameter; $Nt = (\rho c_p)_p D_T(T_w - T_\infty)/\nu(rc_p)_f T_\infty$ is thermophoresis parameter; $Sc = \nu/D_B$ is Schmidt number; and $S = -v_w/\sqrt{(B\nu)}$ is the mass transfer parameter, when $S > 0$ ($v_w < 0$) it indicates the mass suction, and $S < 0$ ($v_w > 0$) it indicates mass injection.

METHOD OF SOLUTION

To solve the nonlinear boundary value problem numerically as given by Eqs.(7) to (9) with associated boundary conditions, Eq.(10), we use the MATLAB bvp4c algorithm. This is achieved by using Eq.(11) to obtain the system of first-order differential equations, which is as follows:

$$f = y_1,\ f' = y_2,\ f'' = y_3,\ \theta = y_4,\ \theta' = y_5,\ \phi = y_6,\ \phi' = y_7, \quad (11)$$

$$y_1' = y_2,\ \ y_2' = y_3,$$

$$y_3' = \frac{1}{1+2\gamma\eta}\left[\left(\frac{\rho_{hnf}/\rho_f}{\mu_{hnf}/\mu_f}\right)(y_2^2 - y_1 y_3) - 2\gamma y_3 + \left(\frac{\sigma_{hnf}/\sigma_f}{\mu_{hnf}/\mu_f}\right)My_2 + Ky_2\right],$$

$$y_4' = y_5,$$

$$y_5' = -\frac{1}{1+2\gamma\eta}\left[\frac{Pr}{k_{hnf}/k_f}\left(\frac{(\rho C_p)_{hnf}}{(\rho C_p)_f}\right)\{y_1 y_5 + (1+2\gamma\eta)\times \times(Nby_5 y_7 + Nty_5 y_5)\} + 2\gamma y_5 + \frac{Pr}{k_{hnf}/k_f}\left(\frac{\sigma_{hnf}}{\sigma_f}\right)MEcy_2 y_2\right],$$

$$y_6' = y_7,$$

$$y_7' = -\frac{1}{1+2\gamma\eta}\left[2\gamma y_7 + Scy_7 y_1 + \left(\frac{Nt}{Nb}\right)2\gamma y_5 + 2\gamma y_5 + \frac{Pr}{k_{hnf}/k_f}\times \times\left(\frac{\sigma_{hnf}}{\sigma_f}\right)MEcy_2 y_2 - \frac{Pr}{k_{hnf}/k_f}\left(\frac{(\rho C_p)_{hnf}}{(\rho C_p)_f}\right)\{y_1 y_5 + (1+2\gamma\eta)\times \times(Nby_5 y_7 + Nty_5 y_5)\}\right],$$

while the code for the boundary condition is given by

$$y_a(1) - S,\ y_a(2) - \lambda,\ y_a(4) - 1,\ Nby_b(7) + Nty_b(5),\ y_b(2),\ y_b(4),\ y_b(6),$$

where: y_a is the condition at $\eta = 0$ and y_b at $\eta = \infty$.

MATLAB's bvp4c function is implemented with suitable values of the governing parameters and the corresponding boundary layer thickness η_∞ until the convergence condition is met, where y_a is the condition at $\eta = 0$, and y_b is the condition at $\eta = \infty$. This approach is based on the finite difference method and ensures a precision of up to 10^{-9}.

Some important characteristics of the flow field

$$C_f = \frac{\mu_{hnf}}{\rho_f U_w^2}\left(\frac{\partial u}{\partial r}\right)_{r=a},\ Nu_x = \frac{xk_{hnf}}{k_f(T_w - T_\infty)}\left(-\frac{\partial T}{\partial r}\right)_{r=a}$$

and

$$Sh_x = \frac{xD_{hnf}}{D_f(C_w - C_\infty)}\left(-\frac{\partial C}{\partial r}\right)_{r=a}. \quad (12)$$

The skin friction coefficient in terms of transformed variables, Eq.(6) and Eq.(12), is obtained as

$$(Re_x)^{1/2} C_f = \frac{\mu_{hnf}}{\mu_f} f''(0), \quad (13)$$

where: $f''(0)$ is obtained using Eq.(7).

The dimensionless expression for Nusselt number is obtained by using Eqs. (6), (8), and Eq.(12) turns out to be

$$(Re_x)^{-1/2} Nu_x = \frac{-k_{hnf}}{k_f}\theta'(0). \quad (14)$$

The dimensionless expression for the Sherwood number in terms of transformed variables, Eq.(6), using Eq.(9) and Eq.(12), turns out to be

$$(Re_x)^{-1/2} Sh_x = \frac{-D_{hnf}}{D_f}\theta'(0), \quad (15)$$

where: $Re_x = U_w(x)x/\nu f$ is Reynolds number. Here, $f''(0)$, $\theta'(0)$ and $\phi'(0)$ can be obtained from Eqs.(7)-(9).

RESULTS AND DISCUSSION

This study aims to examine the heat transfer properties of hydro-magnetic hybrid nanofluid flow around a stretching/shrinking cylinder, considering the influence of thermo-diffusion effects. The hybrid nanofluid is formulated using alumina Al_2O_3 (ϕ_{s1}) and copper Cu (ϕ_{s2}) nanoparticles with water (H_2O) acting as the base fluid. The transformed differential equations obtained by using appropriate similarity transformations are solved numerically by using the bvp4c solver in MATLAB. This approach is employed to determine the velocity, temperature, and concentration profiles of the nanofluid, providing insights into the flow behaviour and heat transfer characteristics. The research also focuses on understanding how key parameters affect the concentration, thermal and fluid flow behaviour in the presence of a magnetic field, permeability parameter, Eckert number, Brownian motion, thermophoresis parameter, Schmidt number, curvature parameter, stretching/shrinking, and suction/injection parameters. The study presents the results of significant physical quantities such as the reduced skin friction coefficient $f''(0)$, reduced Nusselt number $-\theta'(0)$ and reduced Sherwood number $-\phi'(0)$.

Impact on velocity profile $f'(\eta)$

Figure 2 depicts the influence of the magnetic field parameter M on the velocity profile. The Lorentz force, induced by the applied magnetic field, acts as a resistive drag force opposing the fluid motion. As the magnetic field strength increases, this force becomes more significant, restricting fluid movement and thereby reducing the velocity. Consequently, the momentum boundary layer thickness decreases, leading to a more pronounced velocity suppression in the flow region. Effect of permeability parameter K on velocity profile is shown in Fig. 3. From the figure, it is clear that the velocity profile increases with the increasing value of the permeability parameter. The increase in velocity profile with the permeability parameter is primarily due to the effect of porous media resistance. When the permeability of the medium increases, it offers less resistance to fluid flow, allowing the nanofluid to move more freely. This reduction in resistance enhances the velocity profile, leading to an increase in the boundary layer thickness. Figure 4 shows the impact of the stretching parameter λ on the velocity profile. When the stretching parameter increases, the velocity also increases. This is because a higher stretching rate enhances fluid motion near the surface. When the cylinder stretches

($\lambda > 0$) it exerts a pulling force on the nanofluid, accelerating the flow and increasing the velocity within the boundary layer. Suction parameter S affects the velocity profile directly, as the suction parameter increases, the velocity also increases, which is shown in Fig. 5. From Figure 6, it is clear that the enhancement of the copper volume fraction parameter ϕ_{s2} enhances the velocity profile. The inclusion of hybrid nanofluids, such as copper in water as a base fluid, improves their thermal properties, including diffusivity, conductivity, and heat transfer coefficient, which consequently enhances the velocity profile.

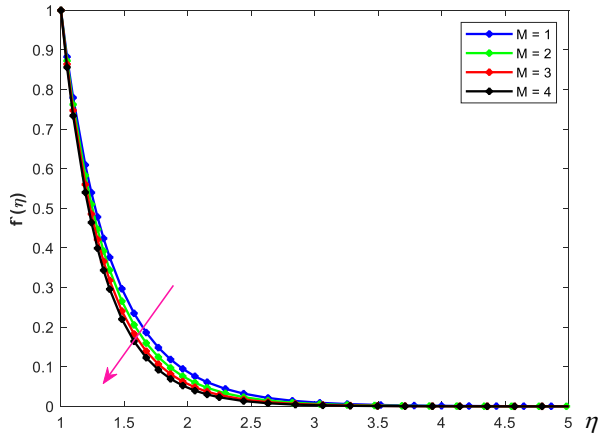

Figure 2. Velocity profiles $f'(\eta)$ for various values of magnetic field parameter M when: $K = 0.5$; $Ec = 0.5$; $S = 2$; $Nb = 0.1$; $Nt = 0.1$; $Pr = 6.2$; $\gamma = 0.1$; $\lambda = 1$; $Sc = 0.5$; $\phi_{s1} = 0.01$; $\phi_{s2} = 0.01$.

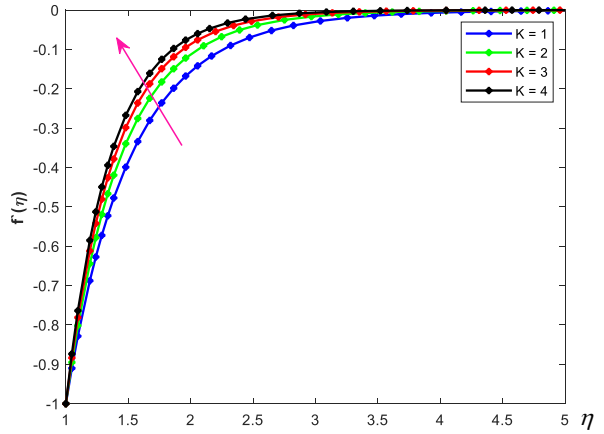

Figure 3. Velocity profiles $f'(\eta)$ for various values of permeability parameter K when: $M = 0.5$; $Ec = 0.5$; $S = 2$; $Nb = 0.1$; $Nt = 0.1$; $Pr = 6.2$; $\gamma = 0.1$; $\lambda = 1$; $Sc = 0.5$; $\phi_{s1} = 0.01$; $\phi_{s2} = 0.01$.

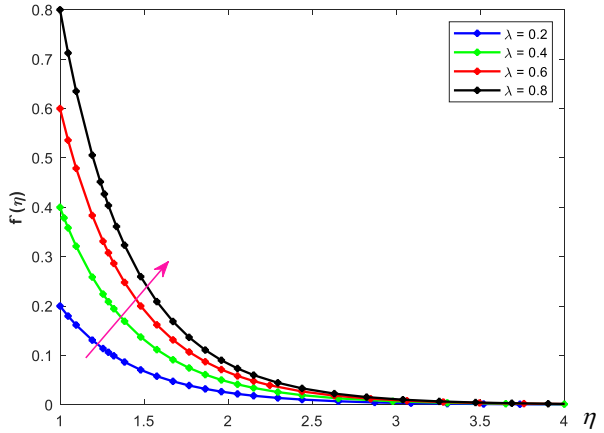

Figure 4. Velocity profiles $f'(\eta)$ for various values of stretching parameter λ when: $M = 0.5$; $Ec = 0.5$; $S = 2$; $Nb = 0.1$; $Nt = 0.1$; $Pr = 6.2$; $\gamma = 0.1$; $K = 0.5$; $Sc = 0.5$; $\phi_{s1} = 0.01$; $\phi_{s2} = 0.01$.

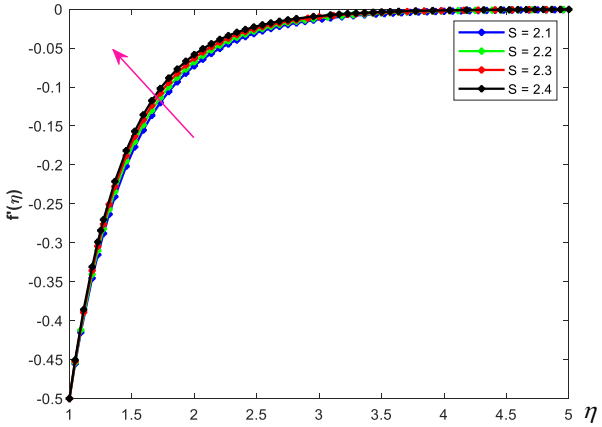

Figure 5. Velocity profiles $f'(\eta)$ for various values of the suction parameter S when: $M = 0.5$; $Ec = 0.5$; $\lambda = -0.5$; $Nb = 0.1$; $Nt = 0.1$; $Pr = 6.2$; $\gamma = 0.1$; $K = 0.5$; $Sc = 0.5$; $\phi_{s1} = 0.01$; $\phi_{s2} = 0.01$.

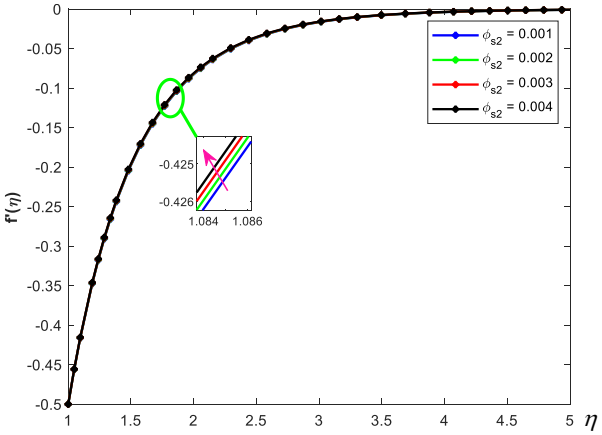

Figure 6. Velocity profiles $f'(\eta)$ for various values of volume fraction parameter ϕ_{s2} when: $M = 0.5$; $Ec = 0.5$; $\lambda = -0.5$; $Nb = 0.1$; $Nt = 0.1$, $S = 2$; $Pr = 6.2$; $\gamma = 0.1$; $K = 0.5$; $Sc = 0.5$; $\phi_{s1} = 0.01$.

Impact on temperature profile $\theta(\eta)$

The influence of the thermophoresis parameter Nt and suction parameter S on dimensionless temperature is shown in Figs. 7 and 8. It is clear from the given figures that the temperature profile increases as thermophoresis parameter and suction parameter increase. The temperature increases due to the effect of thermophoresis, as it drives nanoparticles from hot to cold regions due to temperature gradients. During this process, the nanoparticles affect local thermal conductivity and energy balance. In many situations, this effect promotes the accumulation of nanoparticles in cold regions, reducing heat dissipation and increasing temperature within the fluid. The variation of the temperature profile against the angle of inclination parameter γ is shown in Fig. 9. From the graph, it is noticed that a rise in the angle component enhances the temperature profile. The temperature profile, explained in Figs. 10 and 11, shows that for the enhancement of the aluminium oxide volume fraction parameter ϕ_{s1} and copper volume fraction parameter ϕ_{s2}, the temperature profile $\theta(\eta)$ increases. The hybrid nanofluids improve the thermal conductivity and diffusivity of the flow, which enhances the velocity and temperature profile.

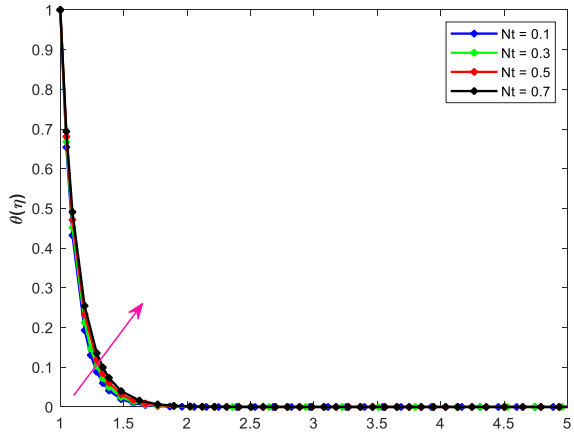

Figure 7. Temperature profiles $\theta(\eta)$ for various values of thermophoresis parameter Nt when: $M = 0.5$; $Ec = 0.5$; $\lambda = -0.5$; $Nb = 0.1$; $S = 2$; $Pr = 6.2$; $\gamma = 0.1$; $K = 0.5$; $Sc = 0.5$; $\phi_{s1} = 0.01$; $\phi_{s2} = 0.01$.

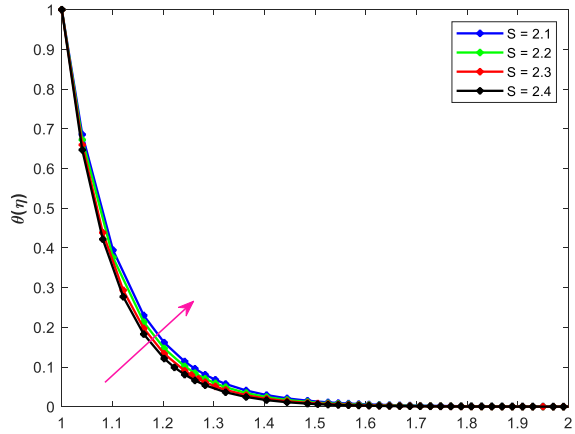

Figure 8. Temperature profiles $\theta(\eta)$ for various values of suction parameter S when: $M = 0.5$; $Ec = 0.5$; $\lambda = -0.5$; $Nb = 0.1$; $Nt = 0.1$; $Pr = 6.2$; $\gamma = 0.1$; $K = 0.5$; $Sc = 0.5$; $\phi_{s1} = 0.01$; $\phi_{s2} = 0.01$.

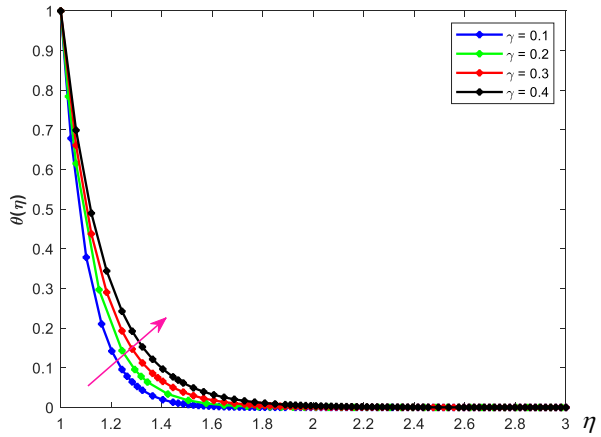

Figure 9. Temperature profiles $\theta(\eta)$ for various values of curvature parameter γ when: $M = 0.5$; $Ec = 0.5$; $\lambda = -1$; $Nb = 0.1$; $Nt = 0.1$; $Pr = 6.2$; $S = 2$; $K = 0.5$; $Sc = 0.5$; $\phi_{s1} = 0.01$; $\phi_{s2} = 0.01$.

Impact on concentration profile $\phi(\eta)$

The influence of curvature parameter γ on concentration profile is shown in Fig. 12. It is found that as the value of the curvature parameter increases, the concentration profile also increases because as γ increases it enhances the boundary layer thickness, which causes the fluid to flow easily. The opposite behaviour is found in the case of Brownian

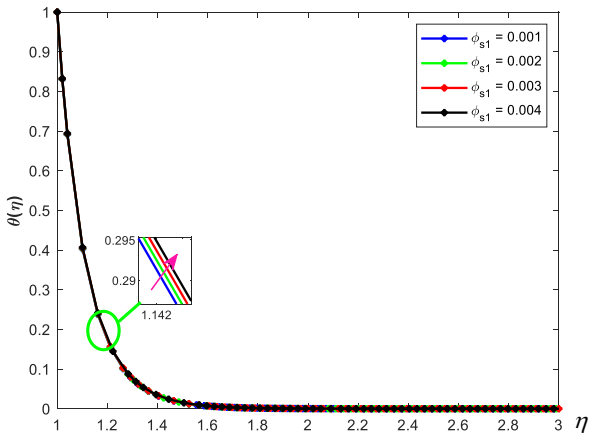

Figure 10. Temperature profiles $\theta(\eta)$ for various values of volume fraction parameter ϕ_{s1} when: $M = 0.5$; $Ec = 0.5$; $\lambda = -0.5$; $Nb = 0.1$; $Nt = 0.1$; $Pr = 6.2$; $\gamma = 0.1$; $S = 2$; $K = 0.5$; $Sc = 0.5$; $\phi_{s2} = 0.01$.

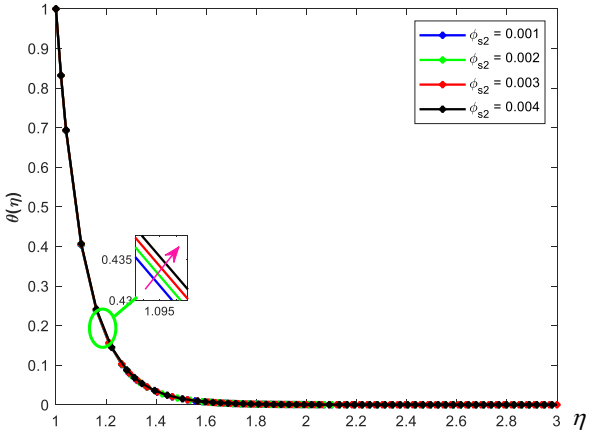

Figure 11. Temperature profiles $\theta(\eta)$ for various values of volume fraction parameter ϕ_{s2} when: $M = 0.5$; $Ec = 0.5$; $\lambda = -0.5$; $Nb = 0.1$; $Nt = 0.1$, $S = 2$; $Pr = 6.2$; $\gamma = 0.1$; $K = 0.5$; $Sc = 0.5$; $\phi_{s1} = 0.01$.

motion parameter Nb on the concentration profile, which is shown in Fig. 13. An increase in values of Nb causes microscopic particles to move erratically and randomly, which leads the boundary layer thickness to decrease, as a result the concentration profile diminishes. Figure 14 shows the impact of thermophoresis parameter Nt on concentration profile. From the figure it is clear that for higher values of Nt the temperature difference between the surrounding region and

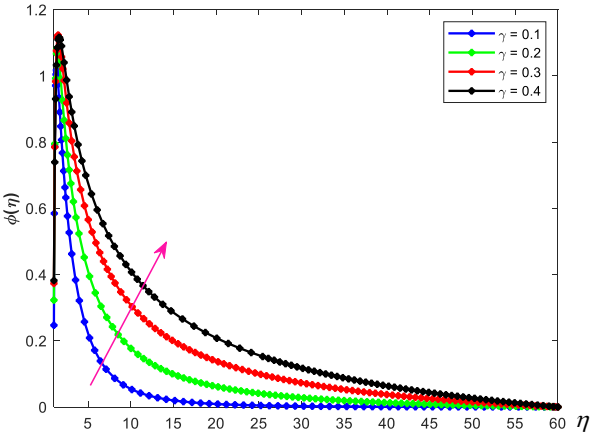

Figure 12. Concentration of nanoparticle profiles $\phi(\eta)$ for various values of curvature parameter γ when: $M = 0.5$; $Ec = 0.5$; $\lambda = -1$; $Nb = 0.1$; $Nt = 0.1$; $Pr = 6.2$; $S = 2$; $K = 0.5$; $Sc = 0.5$; $\phi_{s1} = 0.01$; $\phi_{s2} = 0.01$.

the surface increases, leading to an enhancement in the concentration profile. The influence of Schmidt number *Sc* on concentration profile is present in Fig. 15. From the figure, it is shown that a higher Schmidt number leads to a noticeable reduction in the concentration profile. *Sc* characterises the relationship between momentum diffusivity and mass diffusivity, which indicates how efficiently mass and momentum are transported through diffusion. As the Schmidt number increases, the concentration boundary layer thickness decreases.

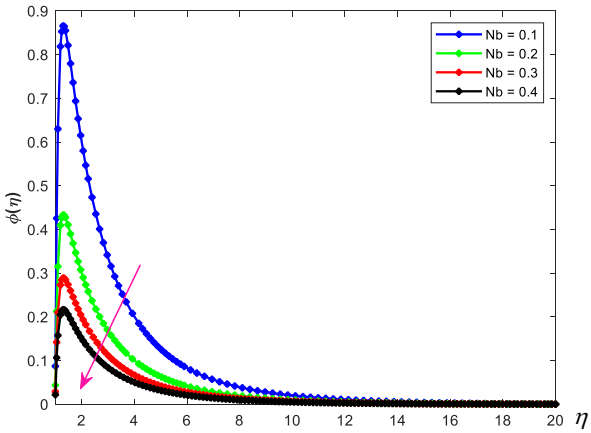

Figure 13. Concentration of nanoparticle profiles $\phi(\eta)$ for various Brownian motion parameter *Nb* when: $M = 0.5$; $Ec = 0.5$; $\lambda = -0.5$; $S = 2$; $Nt = 0.1$; $Pr = 6.2$; $\gamma = 0.1$; $K = 0.5$; $Sc = 0.5$; $\phi_{s1} = 0.01$; $\phi_{s2} = 0.01$.

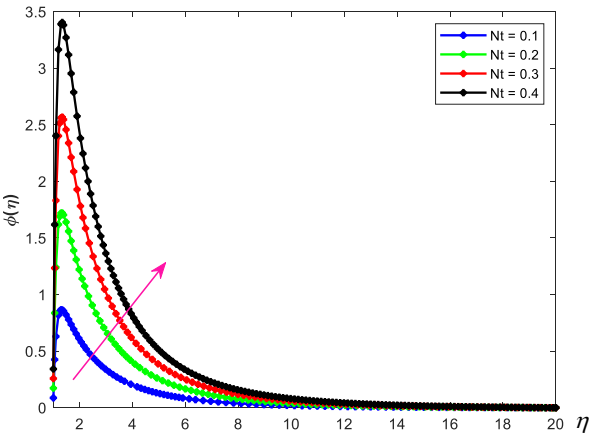

Figure 14. Concentration of nanoparticle profiles $\phi(\eta)$ for various thermophoresis parameter *Nt* when: $M = 0.5$; $Ec = 0.5$; $\lambda = -0.5$; $Nb = 0.1$; $S = 2$; $Pr = 6.2$; $\gamma = 0.1$; $K = 0.5$; $Sc = 0.5$; $\phi_{s1} = 0.01$; $\phi_{s2} = 0.01$.

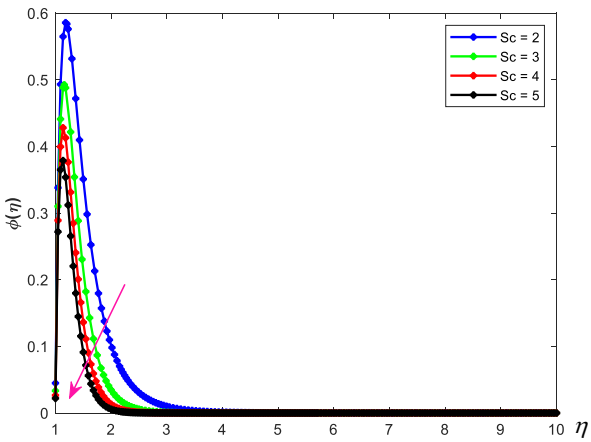

Figure 15. Concentration of nanoparticle profiles $\phi(\eta)$ for various values of Schmidt number *Sc* when: $M = 0.5$; $Ec = 0.5$; $\lambda = -0.5$; $Nb = 0.1$; $Nt = 0.1$; $S = 2$; $Pr = 6.2$; $\gamma = 0.1$; $K = 0.5$; $\phi_{s1} = 0.01$; $\phi_{s2} = 0.01$.

Impact on reduced skin friction coefficient $f''(0)$, reduced Nusselt number $-\theta'(0)$ and reduced Sherwood number $-\phi'(0)$

The influence of the curvature parameter γ on the reduced skin friction coefficient $f''(0)$ for varying values of stretching sheet parameter λ is depicted in Fig. 16. The figure indicates that as the stretching sheet parameter increases, the reduced skin friction coefficient decreases. Additionally, the effect of curvature parameter becomes more prominent for higher values of λ, further contributing to the reduction in $f''(0)$. Figure 17 highlights the effect of suction parameter *S* on the reduced skin friction coefficient. In the case of a shrinking surface ($\lambda < 0$) the coefficient increases with an increasing suction parameter within a specific range, implying that suction enhances the stability of the boundary layer. Conversely, in the stretching surface region ($\lambda > 0$) the reduced skin friction coefficient decreases with increasing suction parameter, signifying a contrasting behaviour between shrinking/stretching surfaces. Figure 18 illustrates that the dimensionless heat transfer rate $-\theta'(0)$ exhibits an increasing trend with both curvature parameter γ and stretch

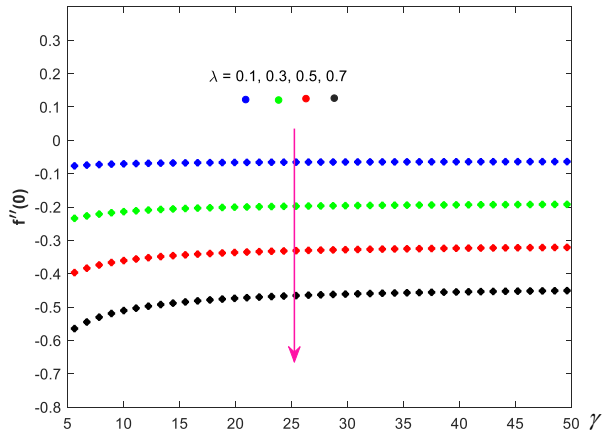

Figure 16. Effect of curvature parameter γ on reduced skin friction coefficient $f''(0)$ with various stretching parameter λ when: $M = 0.5$; $Ec = 0.5$; $S = 2$; $Nb = 0.1$; $Nt = 0.1$; $Pr = 6.2$; $K = 0.5$; $Sc = 0.5$; $\phi_{s1} = 0.01$; $\phi_{s2} = 0.01$.

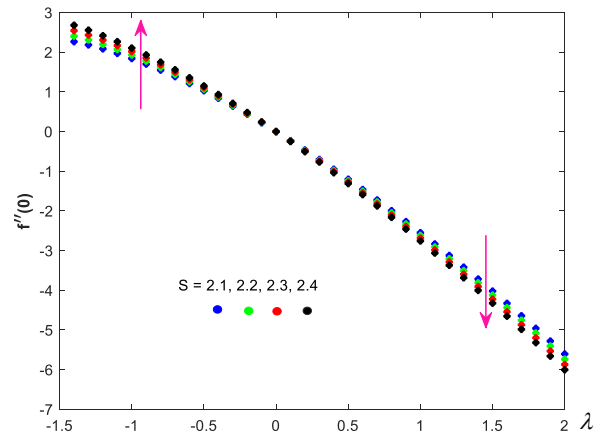

Figure 17. Effect of stretching parameter λ on reduced skin friction coefficient $f''(0)$ with various suction parameter *S* when: $M = 0.5$; $Ec = 0.5$; $Nb = 0.1$; $Nt = 0.1$; $Pr = 6.2$; $\gamma = 0.1$; $K = 0.5$; $Sc = 0.5$; $\phi_{s1} = 0.01$; $\phi_{s2} = 0.01$.

ing sheet parameter λ. This indicates that the presence of curvature enhances heat transfer and higher stretching intensifies this effect, leading to improved thermal energy dissipation.

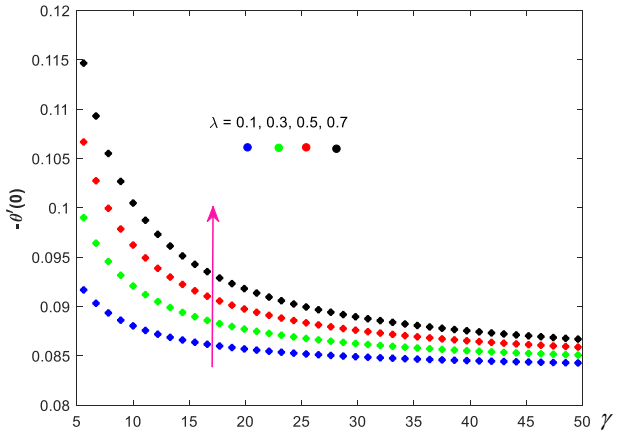

Figure 18. Effect of curvature parameter γ on reduced Nusselt number $-\theta'(0)$ with various stretching parameter λ when: $M = 0.5$; $Ec = 0.5$; $S = 2$; $Nb = 0.1$; $Nt = 0.1$; $Pr = 6.2$; $K = 0.5$; $Sc = 0.5$; $\phi_{s1} = 0.01$; $\phi_{s2} = 0.01$.

Figure 19 demonstrates that the dimensionless mass transfer rate $-\phi'(0)$ decreases with increase in curvature parameter γ as well as the stretching sheet parameter λ. This suggests that higher stretching weakens mass transfer effects, potentially due to changes in the concentration boundary layer thickness caused by stretching and curvature influences.

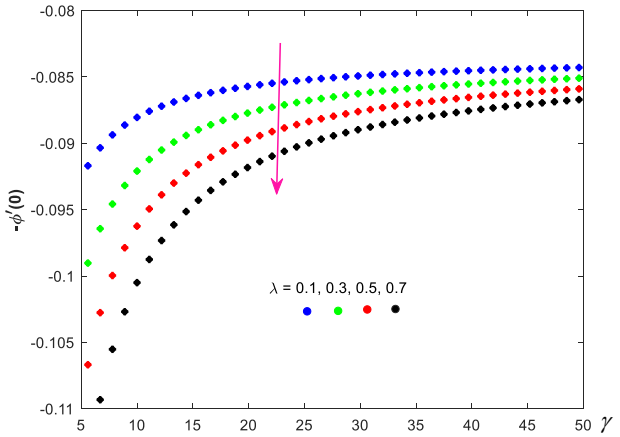

Figure 19. Effect of curvature parameter γ on reduced Sherwood number $-\phi'(0)$ with various stretching parameter λ when: $M = 0.5$; $Ec = 0.5$; $S = 2$; $Nb = 0.1$; $Nt = 0.1$; $Pr = 6.2$; $K = 0.5$; $Sc = 0.5$; $\phi_{s1} = 0.01$; $\phi_{s2} = 0.01$.

Evaluation of the present outcome with the existing results in the literature

To test the validity and accuracy of calculated results, the numerical values of velocity, temperature, and concentration profile for different values of suction parameter S, curvature parameter γ and Schmidt number Sc in the absence of viscous dissipation, magnetic field and permeability effects, which have been compared with the results obtained by Roşca et al. /10/ and expressed in Figs. 20, 21, and 22. The present results are found to be in excellent agreement with previously published results. The consistency between the datasets further reinforces the reliability of the current numerical approach and its suitability for investigating the influence of key physical parameters on flow characteristics.

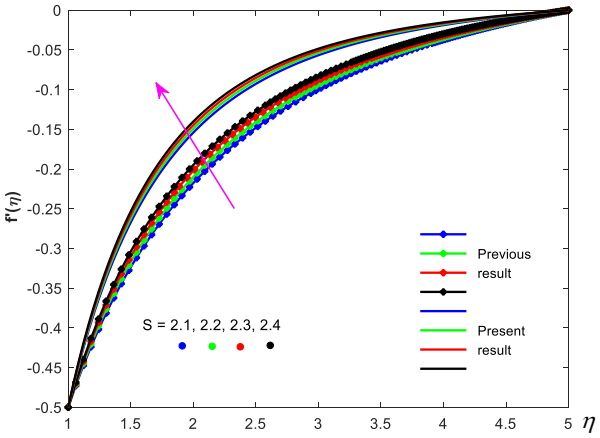

Figure 20. Velocity profiles $f'(\eta)$ for various values of suction parameter S when: $M = 0$; $Ec = 0$; $Nb = 0.1$; $Nt = 0.1$; $\lambda = -0.5$; $Pr = 6.2$; $\gamma = 0.5$; $K = 0$; $Sc = 0.1$; $\phi_{s1} = 0.001$; $\phi_{s2} = 0.001$.

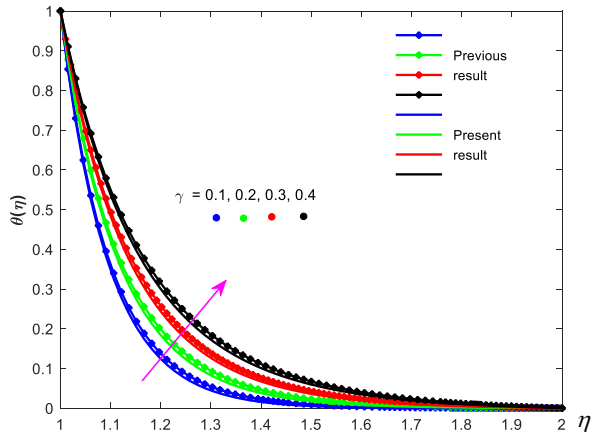

Figure 21. Temperature profiles $\theta(\eta)$ for various values of curvature parameter γ when: $M = 0$; $Ec = 0$; $\lambda = -1$; $Nb = 0.1$; $Nt = 0.1$; $Pr = 6.2$; $S = 2.2$; $K = 0$; $Sc = 0.1$; $\phi_{s1} = 0.001$; $\phi_{s2} = 0.001$.

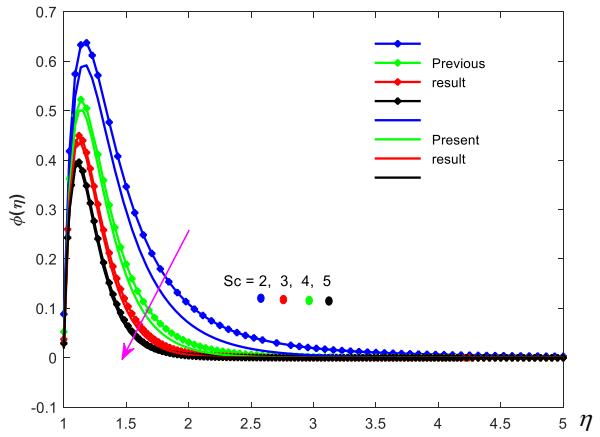

Figure 22. Concentration of nanoparticle profiles $\phi(\eta)$ for various values of Schmidt number Sc when: $M = 0$; $Ec = 0$; $\lambda = -0.5$; $Nb = 0.1$; $Nt = 0.1$; $S = 2.2$; $Pr = 6.2$; $\gamma = 0.5$; $K = 0$; $\phi_{s1} = 0.001$; $\phi_{s2} = 0.001$.

CONCLUSIONS

This study examines the heat transfer characteristics of hydro-magnetic hybrid nanofluid flow around a stretching/shrinking cylinder while considering the effects of thermo-

diffusion. The hybrid nanofluid consists of alumina and copper nanoparticles dispersed in water, which acts as the base fluid. Numerical solutions are obtained using the bvp4c solver in MATLAB. Effects of different parameters on the velocity profile $f'(\eta)$, temperature profile $\theta(\eta)$ as well as the concentration profile $\phi(\eta)$ are analysed. Variations in these profiles due to governing parameters are illustrated through graphical representations. The study also examines the reduced skin friction coefficient $f''(0)$, reduced Nusselt number $-\theta(0)$ and reduced Sherwood number $-\phi(0)$ with different parameters that are presented through graphs. The main outcome of the present analysis is as follows.

The study demonstrates that there is an inverse relationship between velocity profile $f'(\eta)$ and magnetic field parameter M. However, the velocity profile increases with the increment of stretching sheet λ and suction parameter S.

The enhancement of the thermophoresis parameter Nt, curvature parameter γ, suction parameter S and aluminium oxide volume fraction parameter ϕ_{s1} enhance the thermal boundary layer, which implies the temperature profile $\theta(\eta)$ to increase.

Distribution of concentration of nanoparticles increases with increasing value of curvature parameter γ and thermophoresis parameter Nt while opposite behaviour occurs with Brownian motion parameter Nb and Schmidt number Sc.

The reduced skin friction coefficient $f''(0)$ and reduced Sherwood number $-\phi(0)$ decrease as stretching sheet parameter λ and curvature parameter γ increase, whereas reduced Nusselt number $-\theta(0)$ exhibits the opposite trend.

As the value of suction parameter S escalates, the reduced skin friction coefficient $f''(0)$ also escalates, whereas in the case of stretching sheet parameter λ it has the opposite trend, but in the shrinking case, the reduced skin friction also increases.

REFERENCES

1. Choi, S.U.S., Eastman, J.A. (1995), *Enhancing thermal conductivity of fluids with nanoparticles,* ASME Int. Mech. Eng. Congress & Expos., San Francisco, USA, 1995, ASME Fluids Eng. Div. 231: 99-105.
2. Choi, S.U.S., Zhang, Z.G., Yu, W., et al. (2001), *Anomalous thermal conductivity enhancement in nanotube suspensions*, Appl. Phys. Lett. 79(14): 2252-2254. doi: 10.1063/1.1408272
3. Patel, H.E., Das, S.K., Sundararajan, A., et al. (2003), *Thermal conductivities of naked and monolayer-protected metal nanoparticles based nanofluids: Manifestation of anomalous enhancement and chemical effects,* Appl. Phys. Lett. 83(14): 2931-2933. doi: 10.1063/1.1602578
4. Abbas, Z., Rasool, S., Rashidi, M.M. (2015), *Heat transfer analysis due to an unsteady stretching/shrinking cylinder with partial slip condition and suction.* Ain. Shams Eng. J, 6(3): 939-945. doi: 10.1016/j.asej.2015.01.004
5. Hayat, T., Khan, M.I., Waqas, M., Alsaedi, A. (2017), *Newtonian heating effect in nanofluid flow by a permeable cylinder*, Results Phys. 7: 256-262. doi: 10.1016/j.rinp.2016.11.047
6. Mittal, H.V.R., Ray, R.K., AI-Mdallal, Q.M. (2017), *A numerical study of initial flow past an impulsively started rotationally oscillating circular cylinder using a transformation-free HOC scheme*, Phys. Fluids. 29(9): 093603. doi: 10.1063/1.5001731
7. Bilal, M., Sagheer, M., Hussain, S. (2018), *Numerical study of magnetohydrodynamics and thermal radiation on Williamson nanofluid flow over a stretching cylinder with variable thermal conductivity*, Alex. Eng. J, 57(4): 3281-3289. doi: 10.1016/j.aej.2017.12.006
8. Al-Mdallal, Q., Aman, S., Al Fahel, S., et al. (2019), *Numerical study of unsteady flow of a fluid over shrinking long cylinder in a porous medium under magnetic force*, J Nanofluids, 8(7): 1609-1615. doi: 10.1166/jon.2019.1712
9. Khashi'ie, N.S., Arifin, N.M., Hafidzuddin, E.H., Wahi, N. (2019), *Thermally stratified flow of Al_2O_3-Cu/water hybrid nanofluid past a permeable stretching/shrinking circular cylinder*, J Adv. Res. Fluid Mech. Therm. Sci. 63(1): 154-163.
10. Roşca, N.C., Roşca, A.V., Pop, I., Merkin, J.H. (2020), *Nanofluid flow by a permeable stretching/shrinking cylinder*, Heat Mass Transfer, 56: 547-557. doi: 10.1007/s00231-019-02730-x
11. Mishra, A., Kumar, M. (2020), *Velocity and thermal slip effects on MHD nanofluid flow past a stretching cylinder with viscous dissipation and Joule heating*, SN Appl. Sci. 2: 1350. doi: 10.1007/s42452-020-3156-7
12. Khan, M., Rasheed, A. (2021), *Slip velocity and temperature jump effects on molybdenum disulfide MoS_2 and silicon oxide SiO_2 hybrid nanofluid near irregular 3D surface*, Alex. Eng. J, 60(1): 1689-1701. doi: 10.1016/j.aej.2020.11.019
13. Kumar, R.N., Gowda, R.J.P., Prasana, G.D., et al. (2021), *Comprehensive study of thermophoretic diffusion deposition velocity effect on heat and mass transfer of ferromagnetic fluid flow along a stretching cylinder*, Proc. Inst. Mech. Eng., Part E: J Proc. Mech. Eng. 235(5): 1479-1489. doi: 10.1177/09544089211005291
14. Arshad, M., Hussain, A., Hassan, A., et al. (2022), *Thermophoresis and Brownian effect for chemically reacting magnetohydrodynamic nanofluid flow across an exponentially stretching sheet*, Energies, 15(1): 143. doi: 10.3390/en15010143
15. Najib, N., Bachok, N., Dzulkifli, N.F., Pop, I. (2022), *Numerical results on slip effect over an exponentially stretching/shrinking cylinder*, Mathematics, 10(7): 1114. doi: 10.3390/math10071114
16. Sarkar, A., Das, K. (2025), *Magneto-hybrid nanofluid flow with activation energy and chemical reaction through an impermeable stretching elastic cylinder*, Int. J Model. Simul. 45(5): 1560-1572. doi: 10.1080/02286203.2023.2296264
17. Khan, Z., Jan, R., Jawad, M., Hussain, F. (2023), *Radiation heat transfer of hybrid nanofluid stagnation point flow across a stretching porous cylinder*, Therm. Sci. Eng. 6(2): 2595. doi: 10.24294/tse.v6i2.2595
18. Li, S., Shahmir, N., Ramzan, M., et al. (2024), *Thermal inspection of hybrid nanofluid flows over a stretched cylinder at an oblique stagnation point with variable characteristics*, ZAMM-J Appl. Math. Mech. 104(7): e202300837. doi: 10.1002/zamm.202300837